Hydrol. Earth Syst. Sci. Discuss., doi:10.5194/hess-2016-271, 2016
Manuscript under review for journal Hydrol. Earth Syst. Sci.
Published: 30 June 2016

Hydrology and Earth System Sciences
Open Access
Discussions

Response of water vapour D-excess to land-atmosphere interactions in a semi-arid environment

Stephen D. Parkes[1], Matthew F. McCabe[1,2], Alan D. Griffiths[3], Lixin Wang[4], Scott Chambers[3], Ali Ershadi[1,2], Alastair G. Williams[3], Josiah Strauss[2], Adrian Element[3]

[1] Water Desalination and Reuse Centre, King Abdullah University of Science and Technology (KAUST), Jeddah, Saudi Arabia

[2] Department of Civil and Environmental Engineering, University of New South Wales, Sydney, Australia

[3] Australian Nuclear Science and Technology Organization, Sydney, New South Wales, Australia

[4] Department of Earth Sciences, Indiana University–Purdue University Indianapolis (IUPUI), Indianapolis

Corresponding Author: Stephen Parkes, stephen.parkes@kaust.edu.sa

Keywords: Stable isotopes, D-excess, water vapour, land-atmosphere coupling

Hydrol. Earth Syst. Sci. Discuss., doi:10.5194/hess-2016-271, 2016
Manuscript under review for journal Hydrol. Earth Syst. Sci.
Published: 30 June 2016

Hydrology and Earth System Sciences
Open Access
Discussions

Key points:

- Examine the influence of local land-atmosphere coupling on water vapour isotopes
- Diurnal cycle of D-excess in water vapour is determined by an interplay between large scale moisture sources and nocturnal processes
- The D-excess of the evaporation fluxes impose negative forcing on the ambient vapour
- Nocturnal D-excess values are determined by surface exchange and turbulent mixing

Hydrol. Earth Syst. Sci. Discuss., doi:10.5194/hess-2016-271, 2016
Manuscript under review for journal Hydrol. Earth Syst. Sci.
Published: 30 June 2016

Hydrology and Earth System Sciences
Open Access
Discussions

Abstract

The stable isotopic composition of water vapour provides information about moisture sources and processes that is difficult to obtain with traditional measurement techniques. Recently, it has been proposed that the D-excess ($d_v = \delta^2H - 8 \times \delta^{18}O$) of water vapour can provide a diagnostic tracer of continental moisture recycling. However, D-excess exhibits a diurnal cycle that has been observed across a variety of ecosystems and may be influenced by a range of processes beyond regional scale moisture recycling, including local evaporation (ET) fluxes. There is a lack of measurements of D-excess in evaporation (ET) fluxes, which has made it difficult to assess how ET fluxes modify the D-excess in water vapour (d_v). With this in mind, we employed a chamber based approach to directly measure D-excess in ET (d_{ET}) fluxes. We show that ET fluxes imposed a negative forcing on the ambient vapour and could not explain the higher daytime d_v values. The low d_{ET} observed here was sourced from a soil water pool that had undergone an extended drying period, leading to low D-excess of the soil moisture. A strong correlation between daytime d_v and locally measured relative humidity was consistent with an oceanic moisture source, suggesting that remote hydrological processes were the major contributor to daytime d_v variability. During the early evening, ET fluxes into a shallow nocturnal inversion layer caused a lowering of the d_v values near the surface. In addition, transient mixing of vapour with a higher D-excess from above the nocturnal inversion modified these values, causing large within night variability. These results indicate d_{ET} can generally be expected to show large spatial and temporal variability and to depend on the soil moisture state. For long periods between rain events, common in semi-arid environments, ET would be expected to impose negative forcing on the surface d_v. The variability of D-excess in ET fluxes therefore needs to be considered when using d_v to study moisture

Hydrol. Earth Syst. Sci. Discuss., doi:10.5194/hess-2016-271, 2016
Manuscript under review for journal Hydrol. Earth Syst. Sci.
Published: 30 June 2016

Hydrology and Earth System Sciences
Discussions

recycling and during extended dry periods may act as a tracer of the relative humidity of the oceanic moisture source.

1 Introduction

Climate change has the potential to significantly impact surface and atmospheric water budgets. Our best understanding of future exchanges between the atmospheric water cycle and the land surface on a regional to global scale, is likely to be gained through application of numerical models (Decker et al. 2015; Evans and McCabe, 2010; Harding and Snyder, 2012; Wei et al. 2012). Consequently, continual improvement of available models is essential, but is contingent upon ongoing validation and evaluation of model performance over a broad range of landscapes and climate types (McCabe et al. 2016). To do this effectively, a range of datasets are necessary to evaluate the variety of processes represented within these models. Unfortunately, datasets that evaluate land-atmosphere exchanges at the process level are rare.

Water is composed of a number of stable isotopologues that have sufficient abundance to be measured in atmospheric water vapour ($^{1}H_2{}^{16}O$, $^{1}H^{2}H^{16}O$, $^{1}H_2{}^{18}O$ and $^{1}H_2{}^{17}O$). The deviation of the isotope ratios, reported as

$$\delta = \left[\frac{R_{sample}}{R_{VSMOW}} - 1\right]‰ \quad (1)$$

where R is the isotope ratio ($^{2}H/^{1}H$ or $^{18}O/^{16}O$) and VSMOW (Vienna Standard Mean Ocean Water) is the international standard used for reporting water isotope ratios, have potential to evaluate land-atmosphere exchanges by discriminating different processes based on their

Hydrol. Earth Syst. Sci. Discuss., doi:10.5194/hess-2016-271, 2016
Manuscript under review for journal Hydrol. Earth Syst. Sci.
Published: 30 June 2016

Hydrology and Earth System Sciences
Discussions

isotopic signature (Berkelhammer et al. 2013; Lee et al. 2009; Noone et al. 2013; Risi et al. 2013). Isotopic ratios of water vapour (δ^2H and $\delta^{18}O$) can therefore provide information that is either complimentary or even unobtainable when using conventional measurement techniques.

The utility of water isotope ratios for tracing sources of moisture derives from the characteristic isotopic fractionation that occurs when water undergoes a phase change, causing light water molecules to preferentially accumulate in the vapour phase. Soil moisture is typically enriched in heavy isotopes relative to the ocean (Gat, 1996), so water vapour derived from land surface evaporation is expected to have a different isotopic composition to moisture evaporated from the ocean. This has led to a number of studies using stable isotope ratios of precipitation to partition between oceanic and land derived sources (Froehlich et al. 2008; Tian et al. 2001). However, land-atmosphere exchange is not restricted to periods of precipitation, and there are relatively few studies examining the role of land-atmosphere exchange on ambient humidity budgets using stable isotope observations of vapour (Aemisegger et al. 2014; Risi et al. 2013).

In addition to the source of moisture, the magnitude of the isotopic fractionation that occurs as water evaporates is related to the temperature of the liquid surface and the humidity gradient between the evaporating surface and the atmosphere (Craig and Gordon, 1965). The temperature dependent equilibrium exchange between the liquid and vapour is the largest contributor to isotopic fractionation during evaporation, with the fractionation for δ^2H approximately a factor of 8 greater than $\delta^{18}O$. The effect of kinetic fractionation associated with moisture diffusing from the thin laminar layer of vapour in equilibrium with the water surface to the turbulent atmosphere above is influenced by the relative humidity of the atmosphere and wind speed (Merlivat and Jouzel, 1979). The kinetic fractionation factors for δ^2H and $\delta^{18}O$ are similar, causing the ratio of

Hydrol. Earth Syst. Sci. Discuss., doi:10.5194/hess-2016-271, 2016
Manuscript under review for journal Hydrol. Earth Syst. Sci.
Published: 30 June 2016

δ^2H to $\delta^{18}O$ in the evaporating vapour to decrease as kinetic effects increase with decreasing relative humidity. This phenomenon has been observed for evaporative conditions over the Mediterranean sea (Gat et al. 2003; Pfahl and Wernli, 2009) and the Great Lakes in Northern USA (Gat et al. 1994; Vallet-Coulomb et al. 2008).

The D-excess parameter (D-excess = $\delta^2H - 8 \times \delta^{18}O$) (Dansgaard, 1964), quantifies the non-equilibrium isotopic fractionation. A reproducible relationship between the D-excess and relative humidity near the ocean surface has been observed across a wide range of locations (Kurita, 2011; Pfahl and Wernli, 2008; Steen-Larsen et al. 2015; Uemura et al. 2008). Given this, it has been suggested that for precipitation, the D-excess is a good tracer of sea surface evaporative conditions (Masson-Delmotte et al. 2005; Merlivat and Jouzel, 1979). However, this view has recently been challenged due to the role local and regional scale land-atmosphere coupling has in modifying the D-excess of atmospheric humidity over diurnal (Lai and Ehleringer, 2011; Simonin et al. 2014; Welp et al. 2012; Zhao et al. 2014) and synoptic timescales (Aemisegger et al. 2014). As evidence for the role ET plays in modifying the D-excess of water vapour (d_v), a diurnal cycle of the d_v near the land surface across a range of land surface types has been observed (Berkelhammer et al. 2013; Simonin et al. 2014; Welp et al. 2012). The diurnal cycle shows higher values in the day, which has been proposed to be driven by entrainment (Lai and Ehleringer, 2011; Welp et al. 2012), local evapotranspiration sources (Simonin et al. 2014; Zhao et al. 2014) and meteorological conditions affecting the D-excess of the evaporative fluxes (d_{ET}) (Welp et al. 2012; Zhao et al. 2014), coupled with low nocturnal values resulting from equilibrium exchange between liquid and vapour pools (Simonin et al. 2014) and dew fall (Berkelhammer et al. 2013). For synoptic scales, Aemisegger *et al.* (2014) showed that moisture recycling from the land surface had a significant impact on d_v

Hydrol. Earth Syst. Sci. Discuss., doi:10.5194/hess-2016-271, 2016
Manuscript under review for journal Hydrol. Earth Syst. Sci.
Published: 30 June 2016

for *in-situ* measurements in Switzerland. The studies of the d_v diurnal cycles have largely relied on isotopic models to assess the contribution of ET fluxes, but a lack of d_{ET} measurements make it difficult to draw robust conclusions.

The evidence provided by these studies suggest that d_v is a tracer of moisture recycling both on diurnal and synoptic time scales as well as informing upon the dynamics of surface moisture budgets in the atmospheric boundary layer (ABL). However, as outlined by Welp *et al.* (2012), ET and entrainment fluxes both increase as the ABL grows through the previous days residual layer, which can make interpreting the role of local moisture recycling on d_v difficult. To overcome this, Simonin *et al.* (2014) used a trajectory model to simulate the D-excess of vapour evaporated over the ocean. As the d_v was greater than the modelled oceanic moisture source, it was assumed that high daytime values were supported by local ET fluxes. Zhao *et al.* (2014) suggested that since, on cloudy days, no diurnal cycle was observed for the d_v, that ET fluxes played a dominant role. Whilst these studies provide compelling evidence for the role of ET driving the diurnal cycle of d_v, no measurements of d_{ET} were made. To date the only measurements of d_{ET} have been presented by Huang *et al.* (2014) over a maize crop in north west China. Interestingly, their direct measurements conflicted with previous interpretations and showed that the d_{ET} invoked a negative forcing on d_v, even though a strong diurnal cycle of high values in the day and low values at night were observed. In order to better interpret the role of local moisture recycling on the diurnal cycle of d_v, measurements of d_{ET} are required to assess if the negative forcing is consistent in different ecosystems.

The aim of this work is to provide much needed d_{ET} measurements to investigate how ET fluxes modulate the d_v diurnal cycle. To do this, chamber based measurements of the isotopic composition

Hydrol. Earth Syst. Sci. Discuss., doi:10.5194/hess-2016-271, 2016
Manuscript under review for journal Hydrol. Earth Syst. Sci.
Published: 30 June 2016

of the ET fluxes were combined with *in-situ* measurements of water vapour isotope ratios, meteorological and radon concentration observations. The data was collected in a region of the semi-arid Murray Darling basin in south-eastern Australia. These data represent the first such collection of the δ^2H, $\delta^{18}O$ and D-excess in water vapour from this region of Australia. The augmentation of the chamber based measurements with in-situ observations provide a framework to directly assess the role local ET fluxes have has on ambient vapour D-excess.

2 Methods

2.1 Site Description

During the austral autumn of 2011, a field campaign covering the period April 27 to May 11 was conducted at the Baldry Hydrological Observatory (BHO) (-32.87, 148.54, 460 m above sea level) located in the central-west of New South Wales, Australia (Figure 1). The climate of the region is characterised as semi-arid with no clear wet season, a mean annual rainfall of 600 mm, and a mean annual temperature of 24.2°C (source Australian Bureau of Meteorology, 2015, http://www.bom.gov.au/). The BHO grassland flux tower was the central site of the measurements and was located in a natural grassland paddock of dimensions approximately 900m (north-south) by 300m (west-east), with a gentle slope decreasing in elevation by approximately 20 m from southeast to northwest. The flux tower was located 650 m from the road to the south and 200 m from a reforested paddock to the west. The forest site to the west and southwest was reforested in 2001 with *Eucalyptus camaldulensis*, *Eucalyptus crebra* and *Corymbia maculate*. At the time of the campaign these trees were approximately 10 m tall. All other adjacent paddocks and most of the surrounding region had similar surface characteristics to the grassland measurement site.

Hydrol. Earth Syst. Sci. Discuss., doi:10.5194/hess-2016-271, 2016
Manuscript under review for journal Hydrol. Earth Syst. Sci.
Published: 30 June 2016

2.2 Water stable isotope analyses

2.2.1 *In-situ* water vapour calibration and sampling

Stable isotope ratios were monitored using two different *in-situ* analysers. *In-situ* measurements of the isotopic composition in water vapour were made using a Wavelength Scanning Cavity Ring Down Spectrometer (WS-CRDS L115-I, Picarro Inc., Sunnyvale, CA, USA), while the chambers were interfaced to an Off Axis Integrated Cavity Output Spectrometer (OA-ICOS, DLT100, Los Gatos Research (LGR), Mountain View, CA, USA) to determine the isotopic composition of the ET flux. Using an automated continuous flow calibration system (built in-house), we simultaneously determined the calibration coefficients for the two analysers. Calibration experiments were designed to determine the water vapour mixing ratio cross-sensitivity of the isotope ratios and linearity of the δ^2H and $\delta^{18}O$ measurements. Due to logistical constraints, the calibration system was not transported into the field, so corrections were determined by compositing multiple calibration experiments run before and after the campaign.

During the campaign, a second portable calibration system was employed to monitor time dependent drift of the Picarro analyser (CTC HTC-Pal liquid autosampler; LEAP Technologies, Carrboro, NC, USA). Two standards spanning expected water vapour δ^2H (-49.1 and -221.9‰) and $\delta^{18}O$ (-9.17 and -27.57‰) ranges were injected at approximately 18 $mmol.mol^{-1}$ on three occasions during the campaign.

The uncertainty of the isotope measurements of the two analysers was estimated by applying mixing ratio cross-sensitivity and linearity corrections to all calibration measurements collected prior, during and after the campaign. For the Picarro instrument, measurement uncertainty was 0.8, 0.2 and 1.9‰ for δ^2H_v, $\delta^{18}O_v$ and d_v, respectively. No calibrations were performed for the LGR in

Hydrol. Earth Syst. Sci. Discuss., doi:10.5194/hess-2016-271, 2016
Manuscript under review for journal Hydrol. Earth Syst. Sci.
Published: 30 June 2016

Hydrology and Earth System Sciences
Discussions

field, so the measurement uncertainty was estimated from calibration measurements made before and after the campaign, which was 0.9, 0.4 and 3.3‰ for δ^2H, $\delta^{18}O$ and d_v.

Although no calibration experiments were run on the LGR during the campaign, simultaneous *in-situ* measurements were made with the Picarro when chamber measurements were not operated. During the day, the average difference was 0.3 (±1.7), 0.1 (±0.6) and 0.2 (±5.1)‰ for δ^2H, $\delta^{18}O$ and d_v, respectively. At night, while the Picarro was able to maintain a steady cavity and optical housing temperature, the LGR cavity temperature dropped by up to 8°C. In response to the drop in cavity temperature, night time LGR measurements of $\delta^{18}O$ and d_v and to a lesser extent the δ^2H, were physically unrealistic and discarded from subsequent analyses. Morning chamber based measurements were therefore restricted to after 9:00 am, when the LGR cavity temperature had stabilised and *in-situ* measurements were again in agreement with the Picarro.

A schematic diagram illustrating the sampling design for water vapour is shown in Figure 2. Half-hourly vertical profiles of humidity and isotopes were sampled by drawing air to the *in-situ* analyser through 10 mm O.D. PTFE tubing, located at 5 heights on a 7.5 m tower (0.5, 1, 2, 5 and 7.5 m Above Ground Level). The instrument was interfaced to a 5 inlet manifold that enabled sequential sampling of the different heights. A vacuum pump (MV 2 NT, Vacuubrand, Wertheim, Germany) was used to draw air from all inlets to the analyser. To avoid condensation, sample tubes and intakes were wrapped in 15 W m^{-1} heat tape, insulated by Thermobreak pipe and placed inside 100 mm PVC pipe. The sample tube temperature was controlled using a Resistance Thermometer Detector (RTD) coupled to a CAL3300 temperature controller (CAL controls Ltd., Grayslake, IL, USA). The inlets at each height were constructed from inverted funnels with mesh filters. In this study we present block hourly averages of all measurements collected at all heights.

Hydrol. Earth Syst. Sci. Discuss., doi:10.5194/hess-2016-271, 2016
Manuscript under review for journal Hydrol. Earth Syst. Sci.
Published: 30 June 2016

2.2.2 Flux chambers

To separate the isotopic signatures of the ET flux components, flux chambers were deployed on both bare soil and vegetated plots to determine the isotopic signature of the evaporative fluxes. An open chamber was designed with a high volume to footprint ratio to avoid the chamber mixing ratio rapidly reaching the dew point temperature (causing condensation) and to minimise impacts on the evaporation environment. A schematic of the chamber design is shown in Figure 3. Four flanged metal collars were inserted ~10 cm into the soil column two days before the beginning of the campaign. All vegetation was removed from bare soil plots when the metal collars were inserted into the soil. A single chamber cover was constructed of 4 mm G-UVT Plexiglass (Image Plastics, Padstow, Australia), selected for its higher transmittance of UV and blue light. The dimensions of the chamber were 0.1 x 0.1 x 0.8 m (width x length x height), with the inlets and outlets at 0.1 and 0.7 m above the surface, respectively. All sampling tube was 10 mm PTFE. The inlet to the chamber was connected to tubing that drew in air from 1.5 m above the ground surface. The outlet was connected to a flowmeter (VFA-25, Dwyers, Michigan City, IN, USA) that regulated the air flow at 10 $L.min^{-1}$ and was driven by a two-stage diaphragm pump. A T-piece was connected to the LGR, which bled off the required air flow. All tubing between chamber and the analyser were wrapped in heating tape (15 $W\ m^{-2}$) and foam insulation.

To monitor the internal chamber environment, an air temperature and humidity probe (HMP155, Vaisala, Vantaa, Finland) was mounted inside the chamber. To monitor the attenuation of the incoming radiation by the chamber, photosynthetic flux density was measured (LI-190R, Licor, Lincoln, NE, USA) inside and outside the chamber. Ten second averages of the temperature, relative humidity and photosynthetic flux density were stored in a datalogger (CR1000, Campbell

Hydrol. Earth Syst. Sci. Discuss., doi:10.5194/hess-2016-271, 2016
Manuscript under review for journal Hydrol. Earth Syst. Sci.
Published: 30 June 2016

Scientific, Logan, UT, USA). In the supplementary section we use these ancillary measurements to assess the impact of the change in the evaporative conditions caused by the chamber on the isotopic composition of the ET flux. The largest contributor to uncertainty caused by changing the evaporative environment was the temperature, although these affects were small compared to the overall variability of the chamber derived ET isotopic compositions.

2.2.3 Isotopic composition of ET flux from chamber measurements

Using the open chamber system, we determined the isotopic composition of the ET flux using the Keeling mixing model (Keeling, 1958; Wang et al. 2013) given by

$$\delta_{chamber} = q_{BG}\frac{(\delta_{BG}-\delta_{ET})}{q_{chamber}} + \delta_{ET} \quad \textbf{(2)}$$

where q_{BG} is the water vapour mixing ratio entering the chamber through the inlet and δ_{BG} its isotopic composition, $q_{chamber}$ is the mixing ratio in the chamber and δ_{ET} is the isotopic composition of the ET flux. For the Keeling method, δ_{ET} is determined from the intercept of $\delta_{chamber}$ against $1/q_{chamber}$. A key assumption of the Keeling method is that the isotopic composition of the background vapour and the evaporation flux remain constant during the chamber measurements. For chamber measurements longer than 5 minutes, non-linear Keeling plots were commonly observed, indicating a change in isotopic composition of one of the sources of vapour. We therefore restricted the Keeling analysis of the chamber measurement to a maximum of 5 minutes after an increase in the concentration was observed by the analyser. The analysis was also restricted to periods where the H_2O mixing ratio was increasing, so that analysis was generally performed on 2-5 minutes of data. In addition, only chamber measurements where the correlation between $\delta_{chamber}$ and $1/q_{chamber}$ was significant ($p<0.001$) were included in this analysis. A few chamber

Hydrol. Earth Syst. Sci. Discuss., doi:10.5194/hess-2016-271, 2016
Manuscript under review for journal Hydrol. Earth Syst. Sci.
Published: 30 June 2016

243 measurements where obvious non-linearity or very small changes in $q_{chamber}$ occurred were also
244 subjectively removed. Of a total of 105 chamber measurements made from the 4 vegetation plots
245 during the campaign, 99 measurements of the δ^2H_{ET}, and 97 measurements of $\delta^{18}O_{ET}$ and d_{ET} were
246 retained. For the bare soil plots, 84 of the 86 chamber measurements were retained for the δ^2H_{ET},
247 and 77 of the $\delta^{18}O_{ET}$ and d_{ET}. The eight plots were sampled 2 to 4 times each day on all days except
248 the first two days of the campaign, and the 2nd and 5th of May. Sampling was restricted to between
249 9:00 and 17:00 LST (local solar time) as the large temperature dependence of the LGR at low
250 ambient temperatures limited the accuracy of the chamber measurements.

251 Results from the vegetated plots were used to determine the isotopic composition of the ET flux
252 and determine how it influences surface vapour. The bare soil plots were used to determine the
253 isotopic composition of the soil evaporation flux and to provide an estimate of the isotopic
254 composition of the soil water at the evaporation front. The isotopic composition of the water at the
255 evaporation front (δ_L) was determined by rearranging the Craig and Gordon model:

256 $$\delta_L = \frac{\delta_E(1-RH)+RH\ \delta_A+\varepsilon+\varepsilon_k}{\alpha} \quad \textbf{(3)}$$

257 where the isotopic composition of the evaporation flux (δ_E) is taken from the bare soil
258 chamber measurements, relative humidity (RH) normalised to the surface temperature determined
259 from infrared surface temperature measurements (section 2.3), and the ambient vapour isotope
260 composition (δ_A) determined from Picarro *in-situ* measurements. Equilibrium fractionation and
261 enrichment factors (α, $\varepsilon=(\alpha-1)‰$) were calculated from the surface temperature measurements
262 using the equations of Horita and Wesolowski (1994), while the kinetic enrichment factor (ε_k) was
263 determined as in Gat (1996), but using the parameterisation of the exponent of the diffusion

Hydrol. Earth Syst. Sci. Discuss., doi:10.5194/hess-2016-271, 2016
Manuscript under review for journal Hydrol. Earth Syst. Sci.
Published: 30 June 2016

264 coefficients described by Mathieu and Bariac (1996) and the diffusion coefficients determined by
265 Merlivat (1978).

266 **2.2.4 Iso-Forcing of ET**

267 The isotopic composition of the near-surface atmospheric water vapour is modified by surface ET
268 fluxes. The impact of ET fluxes on surface vapour isotopes varies over diurnal timescales with the
269 strength of vertical mixing in the ABL or over synoptic timescales as background moisture
270 conditions change. The magnitude and isotopic composition of the ET flux as well as the amount
271 of water vapour in the atmosphere also have an influence. The ET iso-forcing (I_{ET}) represents a
272 useful quantity to study the influence of ET fluxes on the surface vapour and is defined as:

273 $$I_{ET} = \frac{F_{ET}}{H_2O}(\delta_{ET} - \delta_A) \quad (8)$$

274 where F_{ET} is the ET flux in mol.m^{-2}.s^{-1} taken from an eddy covariance tower, H_2O is the
275 ambient mixing ratio in mol-air.mol-H_2O^{-1} measured by the local meteorological tower, and δ_{ET}
276 and δ_A are the isotopic compositions of the evaporation flux and ambient water vapour,
277 respectively (Lee et al. 2009).

278 For each chamber measurement, a surface iso-forcing was calculated for δ^2H, δ^{18} and D-excess
279 from the determined ET isotopic composition, the hourly averaged ET flux, mixing ratio and δ_A
280 values. The importance of the surface fluxes in modifying surface vapour isotope composition was
281 investigated for diurnal and synoptic timescales.

Hydrol. Earth Syst. Sci. Discuss., doi:10.5194/hess-2016-271, 2016
Manuscript under review for journal Hydrol. Earth Syst. Sci.
Published: 30 June 2016

2.2.5 Plant and soil sampling

Grass samples were collected three times a day for the duration of the campaign. They were sampled randomly within 100 m of the instrumentation. Each sample consisted of approximately 10 grass leaves, which were placed in 12ml Exetainer vials (Labco, Ceredigion, UK). The grass samples were assumed to represent bulk leaf water. Soil samples were collected every 2 days throughout the campaign by sampling from the top 5cm of the soil column. They were collected in 50ml glass bottles. Soil and plant samples were stored in a fridge (4ºC), before they were distilled using a method similar to West *et al*. [2006] and analysed on a Delta V Advantage Isotope Ratio Mass Spectrometer (Thermo Fisher Scientific Corporation, Massachusetts, United States). For δ^2H analysis, water samples were introduced into a H-Device containing a chromium reactor, while for the $\delta^{18}O$ analysis, water samples were equilibrated with CO_2 on a Gas Bench II chromatography column (Thermo Fisher Scientific Corporation, Massachusetts, USA) before being transferred to the IRMS for analysis.

2.3 ET Fluxes and Meteorological measurements

An eddy covariance system comprising a Campbell Scientific 3D sonic anemometer (CSAT-3, Campbell Scientific, Logan, UT, USA) along with a LiCOR 7500 (Li-7500, LiCor Biosciences, Lincoln, NB, USA) analyser was installed at an elevation of 2.5 m. The system was located approximately 10 m from the stable isotope observation tower and sampled at 10 Hz, with flux averages output at 30 minute intervals. The ET fluxes from the eddy covariance tower are used to quantify the Iso-Forcing of ET on the overlying atmosphere.

A meteorological tower was co-located with the eddy covariance system, acting as an aid to the interpretation of measurements. The tower comprised a Kipp and Zonen CNR4 radiometer,

Hydrol. Earth Syst. Sci. Discuss., doi:10.5194/hess-2016-271, 2016
Manuscript under review for journal Hydrol. Earth Syst. Sci.
Published: 30 June 2016

Apogee infrared surface temperature, RIMCO rainguage, Vaisala HMP75C temperature and humidity probe, RM Young wind sentry (wind speed and direction), Huskeflux ground heat flux plate and Vaisala BaroCap barometric pressure sensor. Both meteorological tower data and eddy-covariance data were inspected visually to detect and remove spikes. The low-frequency eddy covariance data (30 minute resolution) were corrected for coordinate rotation (Finnigan et al. 2003) and density effects (Leuning, 2007) using the PyQC software tool (available from code.google.com/p/eddy).

2.4 Radon-222 measurements

The naturally occurring radioactive gas radon (^{222}Rn) is predominantly of terrestrial origin and its only atmospheric sink is through radioactive decay (Zahorowski et al. 2004). The surface flux density of radon is relatively constant in space and time, and since the half-life is much greater than ABL mixing timescales, it is an ideal tracer of the strength of vertical mixing within the ABL (Chambers et al. 2014; Griffiths et al. 2013; Williams et al. 2010). Hourly radon concentrations were measured by an Alpha Guard (Saphymo GmbH, Frankfurt, Germany) placed in a ~20 L enclosure. The enclosure was purged at ~15 L.min^{-1} with a vacuum pump (2107 Series, Thomas, Wisconsin, USA) that sampled from a height of 2 m through 10 mm O.D. PTFE tubing. Radon measurements were used to aid the interpretation of the diurnal variations in vertical mixing (see Griffiths et al. 2013).

3 Results

3.1 Meteorological observations

The two-week campaign was conducted under predominantly calm meteorological conditions. The last rain event was 10 days prior to the campaign, after which clear skies saw the soil dry to a

Hydrol. Earth Syst. Sci. Discuss., doi:10.5194/hess-2016-271, 2016
Manuscript under review for journal Hydrol. Earth Syst. Sci.
Published: 30 June 2016

326 moisture content close to minimum values observed for the site (Figure 4). In the middle of the
327 campaign (May 2nd), a cold front moved across south eastern Australia, producing cloudy
328 conditions and 1.4 mm of precipitation at the site. No change in soil moisture was observed
329 following the rain event over the 0-10 cm soil layer.

330 The wind direction was quite variable over the course of the campaign (see figure S2a and b).
331 Figure S3 shows that from 27th to 30th April, the dominant daytime wind direction was mainly
332 from the east. The predominant wind direction after May 3rd was from the south, except on the
333 7th and 8th when the wind was from the west and with a fetch from the adjacent forest. At other
334 times the fetch did not include the forested site. Daily maximum temperatures on clear days ranged
335 from 16 to 23ºC, whilst night time minimum temperatures fell to between 8 and -4°C. The coldest
336 nights were observed from May 7th onwards, with temperatures falling below zero. On clear nights
337 the surface temperature fell below the dew point temperature as the air reached saturation,
338 indicating dew fall. Apart from the night of the 27-28th April and the cloudy nights between 1st
339 and 3rd May, dew or frost was observed at the site each morning, although dewfall and frost
340 formation was much heavier from the 7th May onwards.

341 Radon concentrations were low during the day, when the convective boundary layer reached its
342 maximum height, with high concentrations at night, when radon emissions from the surface were
343 confined within the shallow nocturnal boundary layer. The accumulation at night was quite
344 variable and indicated a varying degree of nocturnal stability, mixing depth and the occurrence of
345 transient mixing events (Griffiths et al. 2013). There was general agreement between high
346 nocturnal radon concentrations and low wind speeds, but no direct relationship. The lack of a direct
347 relationship indicates that radon can provide additional information about nocturnal mixing and

Hydrol. Earth Syst. Sci. Discuss., doi:10.5194/hess-2016-271, 2016
Manuscript under review for journal Hydrol. Earth Syst. Sci.
Published: 30 June 2016

surface exchange that compliments standard meteorological measurements (Chambers et al. 2015a, 2015b; Williams et al. 2013).

The eddy covariance derived ET fluxes were in general quite low, reflecting the low soil moisture content. The ET flux did show a marked increase the day after the small rain event on May 2nd and noticeably smaller fluxes were observed after the first night that frost was observed. The health of the grass visibly deteriorated over the last 4 days, coinciding with frost formation.

3.2 Relationship between δ^2H and $\delta^{18}O$ of the different water pools

A summary of the isotopic composition of all observed and modelled water pools are presented in Figure 6. The global meteoric water line (MWL) is shown (Craig, 1961), along with the local MWL from the nearby town of Lithgow (Hughes and Crawford, 2013). The local MWL is to the left of the global MWL, illustrating the characteristically high D-excess of precipitation in the region (Crawford et al. 2013; Hughes and Crawford, 2013). The ambient vapour observations align closely with the local MWL, but with a distribution that fell both to the left and right of the local MWL. Alignment between observations and the MWL show that equilibrium fractionation was the dominant process modifying δ^2H and $\delta^{18}O$ in water vapour, while non-equilibrium kinetic processes shift observations away from the MWL and are more easily observed for d_v measurements.

Plant and soil water pools were enriched relative to the vapour and distributed to the right of the MWL, indicating evaporative enrichment. The low slope for vegetation samples is consistent with a number of previous studies across a range of ecosystems (Cernusak et al. 2002; Simonin et al. 2014; Zhao et al. 2014). ET flux isotopic compositions determined from the chambers was

Hydrol. Earth Syst. Sci. Discuss., doi:10.5194/hess-2016-271, 2016
Manuscript under review for journal Hydrol. Earth Syst. Sci.
Published: 30 June 2016

369 enriched relative to the vapour and was distributed to the right of the MWL with a slope of 3.2.
370 Similar isotopic compositions were measured from bare soil and vegetated chambers, with mean
371 values and standard deviations (1σ) of -47.1 (±13) and -50.2 (±11) for δ^2H, -5.03 (±3.8) and -6.3
372 (±2.7)‰ for δ^{18}, and -6.3 (±23) and -0.12 (±15)‰ for D-excess, respectively. Only δ^2H showed a
373 significant difference ($p<0.01$) between the two surface types. The ET isotopic compositions did
374 not show a diurnal cycle, which may result from measurements being restricted mainly to the
375 middle of the day after the large changes in relative humidity and temperature. In addition, no
376 observable trend was seen for synoptic timescales, indicating isotopic compositions of the local
377 moisture source did not vary. Soil water isotopes at the evaporation front ($¢_L$) were much more
378 enriched and had a much lower D-excess (50±12, 31±3.8 and -131±22 ‰ for δ^2H, $\delta^{18}O$ and D-
379 excess) than the average soil moisture between 0 and 5 cm (-15±4.2, 2.6±2.5 and -36±17 ‰ for
380 δ^2H, $\delta^{18}O$ and D-excess). These relatively enriched signatures indicate evaporative enrichment of
381 this water pool.

382 The low slope for the δ^2H vs $\delta^{18}O$ relationship of ET fluxes and liquid pools, illustrates the role of
383 non-equilibrium processes in the evaporation processes. These non-equilibrium processes are
384 likely to have occurred since the last rain event causing the observed enrichment and low D-excess
385 of the soil water pool. The similar isotopic compositions of ET fluxes from bare soil and vegetation
386 chambers indicate that soil evaporation was the dominant process contributing to total ET. The
387 extremely low D-excess values of the moisture at the evaporation front produced fluxes with a D-
388 excess which was low compared to the local ambient vapour. These results illustrate the
389 importance of the soil moisture state for the effect local ET fluxes have on atmospheric vapour D-
390 excess values.

Hydrol. Earth Syst. Sci. Discuss., doi:10.5194/hess-2016-271, 2016
Manuscript under review for journal Hydrol. Earth Syst. Sci.
Published: 30 June 2016

3.3 *In-situ* water vapour isotopes and ET iso-forcing

The observed water vapour mixing ratio and stable isotope composition are shown in Figure 7. The δ^2H and $\delta^{18}O$ variability was similar, reflecting changes in both the synoptic and local meteorology. Leading up to the rain event on May 2nd, relatively moist conditions were observed as air was transported from the warmer ocean off the east coast of Australia (see wind direction in figure S3). After May 5th, drier conditions were observed caused by the lower dew point of air being transported from the colder sea surface to the south of continental Australia. These moisture source regions were confirmed by backward air trajectories calculated using the Stochastic Time-Inverted Lagrangian Transport Model (STILT; Lin *et al.* (2003) not shown). These two time periods are hereinafter referred to as the "wet period" (before May 2nd) and "dry period" (after May 5th). The wet period had relatively moister conditions and coincided with more enriched water isotopes and less diurnal variability. In the later part of the campaign, a reproducible diurnal cycle for δ^2H and $\delta^{18}O$ was observed, characterised by a sharp increase at sunrise before decreasing from mid-morning, when vertical mixing increased until the next sunrise. These observations emphasise the complex relationship between stable isotope observations in water vapour and both local and synoptic scale meteorology.

The dominant feature in the d_v dataset was a robust diurnal cycle of high values in the day and low values at night, consistent with what has been observed across a growing number of locations (Bastrikov et al. 2014; Berkelhammer et al. 2013; Simonin et al. 2014; Welp et al. 2012; Zhao et al. 2014). For the wetter conditions at the start of the campaign, the daytime values were on average lower than those observed for the dry period. Whilst the nocturnal d_v was consistently lower during the night, nocturnal measurements were variable both from night to night and within individual

Hydrol. Earth Syst. Sci. Discuss., doi:10.5194/hess-2016-271, 2016
Manuscript under review for journal Hydrol. Earth Syst. Sci.
Published: 30 June 2016

413 nights. However, no clear difference was observed between nocturnal observations during the wet
414 and dry periods. The differences between the contrasting daytime measurements of the wet and
415 dry periods indicate a role of large scale processes, whilst the lack of contrast in the nocturnal
416 observation show the importance of local processes.

417 The I_{ET} shown in Figure 7 shows large variability on each day, but was always positive for δ^2H
418 and $\delta^{18}O$ and mostly negative for D-excess. I_{ET} is most sensitive to the magnitude of the ET fluxes,
419 producing the greatest forcing on ambient vapour in the middle of the day. Examination of the
420 time series in Figure 7, shows that during the day, δ^2H and $\delta^{18}O$ often decreased, even though the
421 I_{ET} was positive. Likewise, high d_v values observed during the day were associated with negative
422 I_{ET} and the highest daytime d_v observed during the dry period did not correspond to the least
423 negative I_{ET}. These observations illustrates that local ET fluxes were not very important for the
424 trends in d_v over the diurnal cycle or even over synoptic timescales.

425 **3.4 Relationship between water vapour isotopes and local meteorology**

426 The relationships between local meteorological variables and water vapour isotopes were
427 examined to interpret which local processes contributed to the isotope variability. The slope,
428 intercept, coefficient of determination and p-value are shown for the correlations between selected
429 meteorological variables and the isotopes in Table 1. These statistics are shown for both the hourly
430 observations and for the average daytime values (between 11:00 and 16:00 LST). Selecting the
431 daytime measurements removes the effect of the processes associated with the transition between
432 the stable nocturnal and daytime convective boundary layer. It also allows removal of nocturnal
433 periods, where local surface equilibrium exchange and dewfall are known to affect the isotopic
434 composition of ambient vapour. The correlations determined using only measurements in the

Hydrol. Earth Syst. Sci. Discuss., doi:10.5194/hess-2016-271, 2016
Manuscript under review for journal Hydrol. Earth Syst. Sci.
Published: 30 June 2016

middle of the day therefore provide a better indicator of how local meteorology and its isotopic composition modified ambient water vapour isotope ratios from day to day.

For δ^2H, a weak but significant correlation with daytime I_{ET} was observed (R^2=0.45, $p<0.05$). The correlation with I_{ET} potentially indicates that local ET fluxes were important for water vapour δ^2H, but the slope for the relationship was negative. As I_{ET} was positive for δ^2H, the case where local ET fluxes drive daytime δ^2H in water vapour should yield a positive relationship when the ET flux δ^2H is constant. The $\delta^{18}O$ and δ^2H showed weak but significant correlations with air temperature (R^2=0.24 and 0.04, respectively) and the mixing ratio (R^2=0.2 for both isotopes) for hourly measurements, while δ^2H also showed a weak significant correlation with RH (R^2=0.09). The weak relationships with the local meteorology reinforces the role of larger scale precipitation processes and atmospheric mixing that occurs as the moisture is transported to the site.

As already stated, the diurnal cycle was the main mode of variability for d_v, which led to significant correlations with air temperature and RH for the hourly observations. While the local air temperature and RH could modify d_{ET} on diurnal timescales and in turn local d_v, the chamber measurements showed relatively constant d_{ET} over diurnal and synoptic timescales. These correlations may therefore result from the coincident variation of the d_v, RH and air temperature with the daily growth and decay of the ABL.

The daytime average d_v showed significant correlations with the air temperature, RH, ET flux and mixing ratio. The relationship between daytime average ET fluxes and d_v was weak (R^2=0.3) and positive, but as negative iso-forcing was determined for D-excess a negative relationship should have been observed. Likewise, the slope of the linear regression between air temperature and d_v is

Hydrol. Earth Syst. Sci. Discuss., doi:10.5194/hess-2016-271, 2016
Manuscript under review for journal Hydrol. Earth Syst. Sci.
Published: 30 June 2016

456 negative, counter to what theory would predict for local or remote moisture sources. The strongest
457 relationship was observed with daytime RH (R^2 = 0.74), with the negative slope consistent with
458 an expected increase in d_v with RH decreasing at the evaporation source. The strong relationship
459 of d_v with the daytime RH could indicate an important role for the evaporation conditions at remote
460 moisture sources, as is discussed below in Section 4.1.

461 **3.5 Diurnal variability of vapour isotopes**

462 Diurnal composites for the meteorology, radon concentrations and *in-situ* isotope observations are
463 shown in Figure 8, divided into the dry and wet periods defined above. At sunrise (approximately
464 06:30 LST), surface heating leads to initiation of vertical mixing, shown by the topping out of
465 Radon concentrations. The temperature and ET flux start to increase and RH decreases after
466 sunrise. Radon concentrations were still relatively high compared to the middle of day, suggesting
467 that strong convective mixing had not started and that a shallow mixing volume was still in place.
468 ET was injecting water vapour into a relatively shallow mixing volume at this time, which caused
469 a corresponding increase in near-surface humidity. Similarly for δ^2H and $\delta^{18}O$, the observed spike
470 immediately after sunrise was likely caused by ET fluxes with an enriched heavy isotope
471 composition, possibly from re-evaporation of dewfall. During the dry period, when more dewfall
472 occurred, the δ^2H and $\delta^{18}O$ increased more steeply. Assuming the post sunrise inversion layer was
473 of similar depth to the wet period, which radon concentrations indicate was the case, the steeper
474 increase in the stable isotopes can be explained by a greater ET flux from the larger amount of
475 surface condensation into a lower background water vapour volume. As indicated by the rapidly
476 decreasing Radon concentrations, vigorous vertical mixing entraining air from the residual layer
477 of the previous day begins to dilute the early morning fluxes around mid-morning, causing the

Hydrol. Earth Syst. Sci. Discuss., doi:10.5194/hess-2016-271, 2016
Manuscript under review for journal Hydrol. Earth Syst. Sci.
Published: 30 June 2016

478 δ^2H, $\delta^{18}O$ and the mixing ratio to first stabilise and then decrease. ET fluxes rapidly increased
479 during this period, but were not large enough to offset the dilution from the dry air being mixed
480 down from above, or was the iso-forcing of surface fluxes strong enough to stop the depletion of
481 surface humidity isotopes.

482 Similarly to the mixing ratio, δ^2H and $\delta^{18}O$, the d_v increased after sunrise, but the greatest rate of
483 increase was observed slightly later when strong vertical mixing commenced, as shown by the
484 close agreement with the rapid Radon decrease. The iso-forcing for the D-excess was negative,
485 evidence that d_v increased due to encroachment mixing as the new mixed layer grew in depth and
486 not ET fluxes. The dry period showed a greater increase in d_v during the morning transition, which
487 was probably caused by a shift in the d_v of the background water vapour and greater differences
488 between the d_v of the residual and nocturnal layer moisture.

489 In the afternoon, d_v decreased back to values similar to those observed prior to sunrise. At this
490 time, ET fluxes decreased with solar insolation and consequently convective mixing decayed.
491 Radon shows the effect that a reduction in vertical mixing has on the concentration of tracers
492 emitted from the surface. So while ET decreased, small fluxes were still observed well after 18:00
493 when large changes in $\delta^{18}O$ and d_v were observed. Hence, as the I_{ET} was positive and negative for
494 $\delta^{18}O$ and D-excess, respectively, small ET fluxes into a poorly mixed surface layer may have led
495 to these observed changes.

496 During the night, dew fall led to a δ^2H and $\delta^{18}O$ decrease as heavy isotopes were removed in
497 condensing water vapour, which was especially the case during the dry period when greater surface
498 cooling and dew fall was observed. As expected, dew fall did not have a large impact upon the d_v,

Hydrol. Earth Syst. Sci. Discuss., doi:10.5194/hess-2016-271, 2016
Manuscript under review for journal Hydrol. Earth Syst. Sci.
Published: 30 June 2016

as dew formation is an equilibrium process. The composites of both the dry and wet period nocturnal measurements do not show any clear nocturnal trends, remaining stable between the end of the evening transition and the start of the morning transition. However, inspection of individual nights in Figure 8, shows considerable variability, and a regression of the nocturnal d_v measurements with radon concentrations produces a significant negative relationship ($p<0.001$, $R^2 = 0.31$). High radon concentrations are associated with the most stable conditions, which would enhance the effect of surface exchange in the early evening. Low radon concentrations on the other hand, would be associated with periods of atmospheric turbulence in which high d_v air from above the nocturnal inversion is mixed down towards the surface. This process would therefore tend to move d_v back towards the higher values observed during the day.

4 Discussion

As has been previously observed (Steen-Larsen et al. 2013; Welp et al. 2012) and predicted by isotopic models (Gat, 1996), our water vapour δ^2H and $\delta^{18}O$ observations showed different temporal trends than d_v, indicating they are controlled by different atmospheric and hydrological processes. Results presented here illustrate that the diurnal cycle was the dominant mode of variability for d_v, consistent with previous studies for a range of ecosystems (Simonin et al. 2014; Welp et al. 2012; Zhao et al. 2014). However, supported by our chamber based measurements of d_{ET}, interpretation of the data showed that D-excess variability was controlled by local meteorological conditions and surface exchange at night, and larger scale processes in the middle of the day.

Hydrol. Earth Syst. Sci. Discuss., doi:10.5194/hess-2016-271, 2016
Manuscript under review for journal Hydrol. Earth Syst. Sci.
Published: 30 June 2016

Hydrology and Earth System Sciences
Open Access
Discussions

520 **4.1 Daytime d_v variability and remote hydrological processes**

521 As shown in Table 1, the results illustrate a strong correlation between daytime RH and d_v. The
522 slope of the relationship was -0.52‰.%$^{-1}$, which is within the range of slopes determined from
523 coastal locations or shipborne platforms for the Mediterranean or different ocean basins (between
524 -0.43 and -0.53 ‰.%$^{-1}$) (Kurita, 2011; Pfahl and Wernli, 2008; Steen-Larsen et al. 2014, 2015;
525 Uemura et al. 2008). These studies indicate a robust relationship between d_v and RH for
526 evaporation from large water bodies. This strong robust relationship appears not to be restricted to
527 coastal locations or measurements over the ocean surface, as Aemisegger *et al.* (2014) used a
528 trajectory model to investigate continental moisture recycling in Europe, and found a similar
529 relationship between d_v and RH of remote moisture sources during the cold season (-0.57 ‰.%$^{-1}$).
530 However, their warm season observations produced a relationship with a lower slope (-0.19 ‰.%$^{-}$
531 ^{1}). They proposed that because moisture recycling is weakest during winter, d_v retained the
532 signature of the evaporation conditions at the oceanic moisture source. However, moisture
533 recycling increased in the summer and attenuated the relationship. The agreement between their
534 winter measurements and our data indicates that the daytime d_v is at least partly determined by the
535 RH of the oceanic moisture source, and d_v may preserve the signature of evaporation from the
536 ocean surface.

537 Aemisegger *et al.* (2014) proposed that the relationship between the RH and the d_v could be used
538 to determine the D-excess of the moisture source. They argued that when air was saturated with
539 water vapour (when RH is 100%), the d_v is equal to the moisture source, as only equilibrium
540 processes take place and no change in the D-excess between liquid and vapour occurs. By
541 extrapolating the regression between d_v and RH to 100% RH, the D-excess of the moisture source

Hydrol. Earth Syst. Sci. Discuss., doi:10.5194/hess-2016-271, 2016
Manuscript under review for journal Hydrol. Earth Syst. Sci.
Published: 30 June 2016

can be estimated, and gives a value of -8‰. This is approximately the same as the D-excess determined for ocean water off the east coast of Australia by Xu *et al.* (2012) using a global ocean model. In contrast to recent literature (Simonin et al. 2014; Welp et al. 2012; Zhao et al. 2014), this suggests that although the common diurnal cycle was observed, daytime observations are potentially a tracer of oceanic evaporation conditions, in particular RH.

Whilst we have shown a relationship between the RH and d_v consistent with an oceanic vapour source, longer data collections should be examined to evaluate the consistency of the relationship. Datasets collected over longer time periods and over the land surface have not reproduced the strong relationship shown here. For a study of six mid-latitude sites in China and the USA, Welp *et al.* (2012) used much longer datasets and observed slopes between daytime d_v and RH ranging from -0.01 and -0.36‰ $\%^{-1}$. Following on from the warm season interpretation of Aemisegger *et al.* (2014), the lower slopes indicate the importance of moisture recycling from the land surface. Whilst local geographical features such as lakes or seas could alter this relationship, the longer length of their datasets include a greater range of atmospheric conditions and soil moisture states that modify the observed relationship. Here we present data from comparatively quiescent meteorological conditions, where the dominant moisture source is the ocean surrounding the Australian continent. Wetter periods may see an increase in the local and remote moisture recycling that could influence the relationship between local RH and d_v (Aemisegger et al. 2014). However, during dry soil moisture states and for locations such as semi-arid Australia with a relatively close ocean basin, the d_v may indeed be a tracer of oceanic evaporative environments.

The discussion of daytime d_v variability above has not considered the isotopic signature of the entrainment flux from above the convective boundary layer introducing an additional moisture

Hydrol. Earth Syst. Sci. Discuss., doi:10.5194/hess-2016-271, 2016
Manuscript under review for journal Hydrol. Earth Syst. Sci.
Published: 30 June 2016

564 source from the free troposphere. It would be expected to have a depleted isotopic composition
565 compared to the surface and explains the continuing decrease in δ^2H and $\delta^{18}O$ values after midday
566 when convective mixing extends to the top of the capping inversion. The drying trend observed
567 during the day indicates that the entrainment flux was larger than the surface ET fluxes, which has
568 been previously shown using large-eddy simulations (Huang et al. 2011) and observations (Davis
569 et al. 1997). Likewise, the greater entrainment flux would be expected to cause the surface vapour
570 to become depleted in heavy isotopes (Lee et al. 2012).

571 The drying and depleting trend of surface vapour illustrates that entrainment fluxes may influence
572 moisture right down to the surface, but whether this moisture flux impacts on d_v is unclear. In
573 contrast to δ^2H and $\delta^{18}O$ observations, d_v showed no clear trend throughout the middle of the day,
574 but remained high. The expected sign of the iso-forcing of moisture entrained from the free
575 troposphere on d_v is uncertain, as very few measurements exist in the free troposphere. Of the
576 measurements that have been collected, Galewsky and Samuels-Crow (2014) collected *in-situ*
577 observations of water vapour on the Chilean Altiplano and showed periods of extremely high d_v
578 for descending air and lower d_v for ascending air from the ABL. He and Smith (1999) also showed
579 high d_v in the free-troposphere in North America collected from an aircraft platform. These papers
580 suggest moisture entrained from the free troposphere could cause an increase in d_v, but
581 discrimination between the background moisture and free tropospheric moisture is not possible
582 here. Nevertheless, d_v values stabilised during the day and did not show a clear trend until vertical
583 mixing began decaying later in the afternoon, so d_v values of moisture entrained from the free
584 troposphere are not likely to have had a large impact on surface d_v as the two sources of moisture
585 may have had a similar d_v.

Hydrol. Earth Syst. Sci. Discuss., doi:10.5194/hess-2016-271, 2016
Manuscript under review for journal Hydrol. Earth Syst. Sci.
Published: 30 June 2016

4.2 Controls of d_{ET}

From the chamber measurements of d_{ET}, we have shown that the ET fluxes do not contribute to the high values observed during the day. The ET fluxes actually imposed a negative iso-forcing on d_v, which contrasts with interpretations made in previous studies investigating d_v variability on diurnal time scales (Simonin et al. 2014; Zhao et al. 2014). However, it is expected that the sign and magnitude of the D-excess iso-forcing would vary both spatially and temporally.

The measurements presented were collected for a dry soil moisture state with low ET fluxes. The d_{ET} and the associated iso-forcing would be expected to vary with soil moisture state. After a rain event, the soil dries through evaporation of moisture with a D-excess greater than the soil moisture pool, causing the soil moisture D-excess to decrease following a pseudo-Rayleigh process (Barnes and Allison, 1988). The D-excess of moisture at the evaporation front modelled from the bare soil chambers was extremely low (-130 ± 22‰). Assuming the most recent precipitation had a similar D-excess to the intercept of the local MWL (16.2‰), the soil moisture at the evaporation front must have undergone significant evaporative drying. Therefore, immediately after a rainfall event, d_{ET} would be much higher and likely to impose a positive forcing on d_v. As the soil dries, there is likely a tipping point when the ET fluxes switch from positive to negative D-excess iso-forcing. This will have implications for studies attempting to use d_v as a tracer of continental moisture recycling, as the large spatial variability of rainfall and the associated soil moisture state would therefore lead to large spatial and temporal variability for d_{ET}. Although, the strongest moisture recycling is expected for the wettest soils, when d_{ET} is higher and ET fluxes are largest, variability in d_{ET} may still be important.

Hydrol. Earth Syst. Sci. Discuss., doi:10.5194/hess-2016-271, 2016
Manuscript under review for journal Hydrol. Earth Syst. Sci.
Published: 30 June 2016

607 Relative magnitudes of evaporation and transpiration fluxes are important for d_{ET}, as the two
608 processes draw on moisture from different depths within the soil column and are fundamentally
609 different, so fluxes are likely to have different D-excess values. Deeper in the soil column,
610 evaporation has a smaller impact on the soil moisture, so transpiration would be expected to have
611 a higher D-excess than soil evaporation. In agreement with this idea and consistent with the
612 importance of identifying the isotopic composition of the evaporation front outlined by Dubbert et
613 al. (2013), measurements of the D-excess of soil moisture in the 0-5 cm soil layer were much
614 higher than the modelled D-excess for the evaporating front. Similarly we observed slightly higher
615 d_{ET} from vegetated chambers, even when the vegetation was of poor health. It would therefore be
616 expected that for periods of improved vegetation health, increased transpiration fluxes would lead
617 to a higher d_{ET}. The land surface and cover type would therefore constitute an important variable
618 influencing the D-excess of moisture recycling. Further studies investigating how ET partitioning
619 and drying of the soil moisture reservoir following irrigation or precipitation events would lead to
620 a better understanding of how moisture recycling influences the ambient d_v on continental and
621 local scales.

622 **5 Conclusions**

623 To determine how local ET fluxes modified water vapour stable isotopes and in particular the D-
624 excess, in-situ observations were collected in a semi-arid region of south-eastern Australia. The
625 observed diurnal cycle for the D-excess of water vapour, with high values during the day and low
626 values at night, reflected findings from previous analyses. With the addition of chamber based
627 measurements of isotopic compositions in evaporative fluxes, it was shown that the local ET fluxes
628 exhibited a negative forcing on the ambient water vapour D-excess that could not explain the high

Hydrol. Earth Syst. Sci. Discuss., doi:10.5194/hess-2016-271, 2016
Manuscript under review for journal Hydrol. Earth Syst. Sci.
Published: 30 June 2016

daytime values. A strong negative relationship was observed between the locally measured relative humidity and vapour D-excess during the daytime, consistent with relationships observed for oceanic moisture sources. In the evening and night time however, ET fluxes into the shallow nocturnal inversion layer were responsible for lowering the D-excess of water vapour near the surface. In addition, a negative correlation between D-excess and radon concentrations at night indicated that transient nocturnal mixing events shifted the D-excess back towards the higher values observed during the day, with the most stable (least turbulent) nights producing the lowest D-excess values. In the morning, encroachment and entrainment of high D-excess air from above caused D-excess of the surface vapour to increase back to the synoptic values.

Overall, it was found that the magnitude of the D-excess diurnal cycle was controlled predominantly by interplay between synoptic forcing and local ABL processes and was modified further by nocturnal surface exchange processes and turbulent mixing. The low D-excess of the ET fluxes determined from flux chambers in this study illustrated that the impact of large scale moisture recycling may be both spatially and temporally variable, depending on the soil moisture state. This has implications for studies using D-excess to investigate moisture recycling.

6 Acknowledgements

Stephen Parkes was supported by the Atmospheric Mixing and Pollution Transport (AMPT) project at the Australian Nuclear Science and Technology Organization (ANSTO). The Baldry Hydrological Observatory field campaign was supported by Australian Research Council Discovery grants DP0987478 and DP120104718. Matthew McCabe and Stephen Parkes acknowledge the support of the King Abdullah University of Science and Technology. We thank Peter Graham, Cecilia Azcurra, Dr. Jin Wang and Yingzhe Cai for their assistance during the

651 campaign. We also appreciate the support of Diana and Jason Tremain for access to the Baldry
652 Hydrological Observatory and surrounding farmland, Chris Dimovski for performing plant and
653 soil water extractions, and Barbara Neklapilova analysis of plant and soil water samples.

654 For access to the data used in this paper contact Dr Stephen Parkes by email
655 (stephen.parkes@kaust.edu.sa).

656

657

658 **7 References**

659 Aemisegger, F., Pfahl, S., Sodemann, H., Lehner, I., Seneviratne, S. I. and Wernli, H.: Deuterium
660 excess as a proxy for continental moisture recycling and plant transpiration, Atmos. Chem. Phys.,
661 14(8), 4029–4054, doi:10.5194/acp-14-4029-2014, 2014.

662 Barnes, C. J. and Allison, G. B.: Tracing of water movement in the unsaturated zone using stable
663 isotopes of hydrogen and oxygen, J. Hydrol., 100(1-3), 143–176, doi:10.1016/0022-
664 1694(88)90184-9, 1988.

665 Bastrikov, V., Steen-Larsen, H. C., Masson-Delmotte, V., Gribanov, K., Cattani, O., Jouzel, J. and
666 Zakharov, V.: Continuous measurements of atmospheric water vapour isotopes in western Siberia
667 (Kourovka), Atmos. Meas. Tech., 7(6), 1763–1776, doi:10.5194/amt-7-1763-2014, 2014.

668 Berkelhammer, M., Hu, J., Bailey, A., Noone, D. C., Still, C. J., Barnard, H., Gochis, D., Hsiao,
669 G. S., Rahn, T. and Turnipseed, A.: The nocturnal water cycle in an open-canopy forest, J.
670 Geophys. Res. Atmos., 118(17), 10,210–225,242, doi:10.1002/jgrd.50701, 2013.

671 Cernusak, L. A., Pate, J. S. and Farquhar, G. D.: Diurnal variation in the stable isotope composition
672 of water and dry matter in fruiting Lupinus angustifolius under field conditions, Plant. Cell
673 Environ., 25(7), 893–907, doi:10.1046/j.1365-3040.2002.00875.x, 2002.

674 Chambers, S. D., Wang, F., Williams, A. G., Xiaodong, D., Zhang, H., Lonati, G., Crawford, J.,
675 Griffiths, A. D., Ianniello, A. and Allegrini, I.: Quantifying the influences of atmospheric stability
676 on air pollution in Lanzhou, China, using a radon-based stability monitor, Atmos. Environ., 107,
677 233–243, doi:10.1016/j.atmosenv.2015.02.016, 2015a.

678 Chambers, S. D., Williams, A. G., Crawford, J. and Griffiths, A. D.: On the use of radon for
679 quantifying the effects of atmospheric stability on urban emissions, Atmos. Chem. Phys. Discuss.,
680 14(18), 25411–25452, doi:10.5194/acpd-14-25411-2014, 2014.

681 Chambers, S. D., Williams, A. G., Crawford, J. and Griffiths, A. D.: On the use of radon for
682 quantifying the effects of atmospheric stability on urban emissions, Atmos. Chem. Phys., 15(3),
683 1175–1190, doi:10.5194/acp-15-1175-2015, 2015b.

684 Craig, H.: Isotopic Variations in Meteoric Waters, Sci. , 133 (3465), 1702–1703,
685 doi:10.1126/science.133.3465.1702, 1961.

686 Craig, H. and Gordon, L. I.: Deuterium and oxygen-18 variations in the ocean and marine
687 atmosphere, in Stable isotopes in oceanographic studies and paleotemperatures, Proceedings,
688 Spoleto, Italy., edited by E. Tongiogi, pp. 9–130, Pisa, Italy., 1965.

689 Crawford, J., Hughes, C. E. and Parkes, S. D.: Is the isotopic composition of event based
690 precipitation driven by moisture source or synoptic scale weather in the Sydney Basin, Australia?,
691 J. Hydrol., 507(0), 213–226, doi:http://dx.doi.org/10.1016/j.jhydrol.2013.10.031, 2013.

692 Dansgaard, W.: Stable isotopes in precipitation, Tellus, 16(4), 436–468, doi:10.1111/j.2153-
693 3490.1964.tb00181.x, 1964.

694 Davis, K. J., Lenschow, D. H., Oncley, S. P., Kiemle, C., Ehret, G., Giez, A. and Mann, J.: Role
695 of entrainment in surface-atmosphere interactions over the boreal forest, J. Geophys. Res. Atmos.,
696 102(D24), 29219–29230, doi:10.1029/97JD02236, 1997.

697 Decker, M., Pitman, A. and Evans, J.: Diagnosing the seasonal land–atmosphere correspondence
698 over northern Australia: dependence on soil moisture state and correspondence strength definition,
699 Hydrol. Earth Syst. Sci., 19(8), 3433–3447, doi:10.5194/hess-19-3433-2015, 2015.

700 Dubbert, M., Cuntz, M., Piayda, A., Maguás, C. and Werner, C.: Partitioning evapotranspiration
701 – Testing the Craig and Gordon model with field measurements of oxygen isotope ratios of
702 evaporative fluxes, J. Hydrol., 496, 142–153, doi:10.1016/j.jhydrol.2013.05.033, 2013.

703 Evans, J. P. and McCabe, M. F.: Regional climate simulation over Australia's Murray-Darling
704 basin: A multitemporal assessment, J. Geophys. Res. Atmos., 115(D14), n/a–n/a,
705 doi:10.1029/2010JD013816, 2010.

706 Finnigan, J. J., Clement, R., Malhi, Y., Leuning, R. and Cleugh, H. A.: A Re-Evaluation of Long-
707 Term Flux Measurement Techniques Part I: Averaging and Coordinate Rotation, Boundary-Layer
708 Meteorol., 107(1), 1–48, doi:10.1023/A:1021554900225, 2003.

709 Froehlich, K., Kralik, M., Papesch, W., Rank, D., Scheifinger, H. and Stichler, W.: Deuterium
710 excess in precipitation of Alpine regions – moisture recycling, Isotopes Environ. Health Stud.,
711 44(1), 61–70, doi:10.1080/10256010801887208, 2008.

712 Galewsky, J. and Samuels-Crow, K.: Summertime Moisture Transport to the Southern South
713 American Altiplano: Constraints from In Situ Measurements of Water Vapor Isotopic
714 Composition, J. Clim., 28(7), 2635–2649, doi:10.1175/JCLI-D-14-00511.1, 2014.

715 Gat, J. R.: OXYGEN AND HYDROGEN ISOTOPES IN THE HYDROLOGIC CYCLE, Annu.
716 Rev. Earth Planet. Sci., 24(1), 225–262, doi:10.1146/annurev.earth.24.1.225, 1996.

717 Gat, J. R., Bowser, C. J. and Kendall, C.: The contribution of evaporation from the Great Lakes to
718 the continental atmosphere: estimate based on stable isotope data, Geophys. Res. Lett., 21(7), 557–
719 560, doi:10.1029/94GL00069, 1994.

720 Gat, J. R., Klein, B., Kushnir, Y., Roether, W., Wernli, H., Yam, R. and Shemesh, A.: Isotope

composition of air moisture over the Mediterranean Sea: an index of the air–sea interaction pattern, Tellus B, 55(5), 953–965, doi:10.1034/j.1600-0889.2003.00081.x, 2003.

Griffiths, A. D., Parkes, S. D., Chambers, S. D., McCabe, M. F. and Williams, A. G.: Improved mixing height monitoring through a combination of lidar and radon measurements, Atmos. Meas. Tech., 6(2), 207–218, doi:10.5194/amt-6-207-2013, 2013.

Harding, K. J. and Snyder, P. K.: Modeling the Atmospheric Response to Irrigation in the Great Plains. Part I: General Impacts on Precipitation and the Energy Budget, J. Hydrometeorol., 13(6), 1667–1686, doi:10.1175/JHM-D-11-098.1, 2012.

He, H. and Smith, R. B.: Stable isotope composition of water vapor in the atmospheric boundary layer above the forests of New England, J. Geophys. Res. Atmos., 104(D9), 11657–11673, doi:10.1029/1999JD900080, 1999.

Horita, J. and Wesolowski, D. J.: Liquid-vapor fractionation of oxygen and hydrogen isotopes of water from the freezing to the critical temperature, Geochim. Cosmochim. Acta, 58(16), 3425–3437, doi:http://dx.doi.org/10.1016/0016-7037(94)90096-5, 1994.

Huang, J., Lee, X. and Patton, E. G.: Entrainment and budgets of heat, water vapor, and carbon dioxide in a convective boundary layer driven by time-varying forcing, J. Geophys. Res. Atmos., 116(D6), D06308, doi:10.1029/2010JD014938, 2011.

Huang, L. and Wen, X.: Temporal variations of atmospheric water vapor δD and δ18O above an arid artificial oasis cropland in the Heihe River Basin, J. Geophys. Res. Atmos., 119(19), 2014JD021891, doi:10.1002/2014JD021891, 2014.

Hughes, C. E. and Crawford, J.: Spatial and temporal variation in precipitation isotopes in the Sydney Basin, Australia, J. Hydrol., 489(0), 42–55, doi:http://dx.doi.org/10.1016/j.jhydrol.2013.02.036, 2013.

Keeling, C. D.: The concentration and isotopic abundances of atmospheric carbon dioxide in rural areas, Geochim. Cosmochim. Acta, 13(4), 322–334, doi:10.1016/0016-7037(58)90033-4, 1958.

Kurita, N.: Origin of Arctic water vapor during the ice-growth season, Geophys. Res. Lett., 38(2), n/a–n/a, doi:10.1029/2010GL046064, 2011.

Lai, C.-T. and Ehleringer, J.: Deuterium excess reveals diurnal sources of water vapor in forest air, Oecologia, 165(1), 213–223, doi:10.1007/s00442-010-1721-2, 2011.

Lee, X., Griffis, T. J., Baker, J. M., Billmark, K. A., Kim, K. and Welp, L. R.: Canopy-scale kinetic fractionation of atmospheric carbon dioxide and water vapor isotopes, Global Biogeochem. Cycles, 23(1), GB1002, doi:10.1029/2008GB003331, 2009.

Lee, X., Huang, J. and Patton, E.: A Large-Eddy Simulation Study of Water Vapour and Carbon Dioxide Isotopes in the Atmospheric Boundary Layer, Boundary-Layer Meteorol., 145(1), 229–248, doi:10.1007/s10546-011-9631-3, 2012.

Leuning, R.: The correct form of the Webb, Pearman and Leuning equation for eddy fluxes of trace gases in steady and non-steady state, horizontally homogeneous flows, Boundary-Layer Meteorol., 123(2), 263–267, doi:10.1007/s10546-006-9138-5, 2007.

Lin, J. C., Gerbig, C., Wofsy, S. C., Andrews, A. E., Daube, B. C., Davis, K. J. and Grainger, C. A.: A near-field tool for simulating the upstream influence of atmospheric observations: The

761 Stochastic Time-Inverted Lagrangian Transport (STILT) model, J. Geophys. Res., 108, 4493,
762 doi:10.1029/2002JD003161, 2003.

763 Masson-Delmotte, V., Jouzel, J., Landais, A., Stievenard, M., Johnsen, S. J., White, J. W. C.,
764 Werner, M., Sveinbjornsdottir, A. and Fuhrer, K.: GRIP Deuterium Excess Reveals Rapid and
765 Orbital-Scale Changes in Greenland Moisture Origin, Sci. , 309 (5731), 118–121,
766 doi:10.1126/science.1108575, 2005.

767 Mathieu, R. and Bariac, T.: A numerical model for the simulation of stable isotope profiles in
768 drying soils, J. Geophys. Res. Atmos., 101(D7), 12685–12696, doi:10.1029/96JD00223, 1996.

769 McCabe, M. F., Ershadi, A., Jimenez, C., Miralles, D. G., Michel, D. and Wood, E. F.: The
770 GEWEX LandFlux project: evaluation of model evaporation using tower-based and globally
771 gridded forcing data, Geosci. Model Dev., 9(1), 283–305, doi:10.5194/gmd-9-283-2016, 2016.

772 Merlivat, L.: Molecular diffusivities of H[sub 2] [sup 16]O, HD[sup 16]O, and H[sub 2] [sup 18]O
773 in gases, J. Chem. Phys., 69(6), 2864, doi:10.1063/1.436884, 1978.

774 Merlivat, L. and Jouzel, J.: Global climatic interpretation of the deuterium-oxygen 18 relationship
775 for precipitation, J. Geophys. Res. Ocean., 84(C8), 5029–5033, doi:10.1029/JC084iC08p05029,
776 1979.

777 Noone, D., Risi, C., Bailey, A., Berkelhammer, M., Brown, D. P., Buenning, N., Gregory, S.,
778 Nusbaumer, J., Schneider, D., Sykes, J., Vanderwende, B., Wong, J., Meillier, Y. and Wolfe, D.:
779 Determining water sources in the boundary layer from tall tower profiles of water vapor and
780 surface water isotope ratios after a snowstorm in Colorado, Atmos. Chem. Phys., 13(3), 1607–
781 1623, doi:10.5194/acp-13-1607-2013, 2013.

782 Pfahl, S. and Wernli, H.: Air parcel trajectory analysis of stable isotopes in water vapor in the
783 eastern Mediterranean, J. Geophys. Res. Atmos., 113(D20), n/a–n/a, doi:10.1029/2008JD009839,
784 2008.

785 Pfahl, S. and Wernli, H.: Lagrangian simulations of stable isotopes in water vapor: An evaluation
786 of nonequilibrium fractionation in the Craig-Gordon model, J. Geophys. Res. Atmos., 114(D20),
787 D20108, doi:10.1029/2009JD012054, 2009.

788 Risi, C., Noone, D., Frankenberg, C. and Worden, J.: Role of continental recycling in intraseasonal
789 variations of continental moisture as deduced from model simulations and water vapor isotopic
790 measurements, Water Resour. Res., 49(7), 4136–4156, doi:10.1002/wrcr.20312, 2013.

791 Simonin, K. A., Link, P., Rempe, D., Miller, S., Oshun, J., Bode, C., Dietrich, W. E., Fung, I. and
792 Dawson, T. E.: Vegetation induced changes in the stable isotope composition of near surface
793 humidity, Ecohydrology, 7(3), 936–949, doi:10.1002/eco.1420, 2014.

794 Steen-Larsen, H. C., Johnsen, S. J., Masson-Delmotte, V., Stenni, B., Risi, C., Sodemann, H.,
795 Balslev-Clausen, D., Blunier, T., Dahl-Jensen, D., Ellehøj, M. D., Falourd, S., Grindsted, A.,
796 Gkinis, V., Jouzel, J., Popp, T., Sheldon, S., Simonsen, S. B., Sjolte, J., Steffensen, J. P., Sperlich,
797 P., Sveinbjörnsdóttir, A. E., Vinther, B. M. and White, J. W. C.: Continuous monitoring of summer
798 surface water vapor isotopic composition above the Greenland Ice Sheet, Atmos. Chem. Phys.,
799 13(9), 4815–4828, doi:10.5194/acp-13-4815-2013, 2013.

800 Steen-Larsen, H. C., Sveinbjörnsdottir, A. E., Jonsson, T., Ritter, F., Bonne, J.-L., Masson-
801 Delmotte, V., Sodemann, H., Blunier, T., Dahl-Jensen, D. and Vinther, B. M.: Moisture sources

802 and synoptic to seasonal variability of North Atlantic water vapor isotopic composition, J.
803 Geophys. Res. Atmos., 120(12), 2015JD023234, doi:10.1002/2015JD023234, 2015.

804 Steen-Larsen, H. C., Sveinbjörnsdottir, A. E., Peters, A. J., Masson-Delmotte, V., Guishard, M.
805 P., Hsiao, G., Jouzel, J., Noone, D., Warren, J. K. and White, J. W. C.: Climatic controls on water
806 vapor deuterium excess in the marine boundary layer of the North Atlantic based on 500 days of
807 in situ, continuous measurements, Atmos. Chem. Phys., 14(15), 7741–7756, doi:10.5194/acp-14-
808 7741-2014, 2014.

809 Tian, L., Masson-Delmotte, V., Stievenard, M., Yao, T. and Jouzel, J.: Tibetan Plateau summer
810 monsoon northward extent revealed by measurements of water stable isotopes, J. Geophys. Res.
811 Atmos., 106(D22), 28081–28088, doi:10.1029/2001JD900186, 2001.

812 Uemura, R., Matsui, Y., Yoshimura, K., Motoyama, H. and Yoshida, N.: Evidence of deuterium
813 excess in water vapor as an indicator of ocean surface conditions, J. Geophys. Res. Atmos.,
814 113(D19), n/a–n/a, doi:10.1029/2008JD010209, 2008.

815 Vallet-Coulomb, C., Gasse, F. and Sonzogni, C.: Seasonal evolution of the isotopic composition
816 of atmospheric water vapour above a tropical lake: Deuterium excess and implication for water
817 recycling, Geochim. Cosmochim. Acta, 72(19), 4661–4674, doi:10.1016/j.gca.2008.06.025, 2008.

818 Wang, L., Niu, S., Good, S. P., Soderberg, K., McCabe, M. F., Sherry, R. A., Luo, Y., Zhou, X.,
819 Xia, J. and Caylor, K. K.: The effect of warming on grassland evapotranspiration partitioning using
820 laser-based isotope monitoring techniques, Geochim. Cosmochim. Acta, 111, 28–38,
821 doi:10.1016/j.gca.2012.12.047, 2013.

822 Wei, J., Dirmeyer, P. A., Wisser, D., Bosilovich, M. G. and Mocko, D. M.: Where Does the
823 Irrigation Water Go? An Estimate of the Contribution of Irrigation to Precipitation Using MERRA,
824 J. Hydrometeorol., 14(1), 275–289, doi:10.1175/JHM-D-12-079.1, 2012.

825 Welp, L. R., Lee, X., Griffis, T. J., Wen, X.-F., Xiao, W., Li, S., Sun, X., Hu, Z., Val Martin, M.
826 and Huang, J.: A meta-analysis of water vapor deuterium-excess in the midlatitude atmospheric
827 surface layer, Global Biogeochem. Cycles, 26(3), GB3021, doi:10.1029/2011GB004246, 2012.

828 Williams, A. G., Chambers, S. and Griffiths, A.: Bulk Mixing and Decoupling of the Nocturnal
829 Stable Boundary Layer Characterized Using a Ubiquitous Natural Tracer, Boundary-Layer
830 Meteorol., 149(3), 381–402, doi:10.1007/s10546-013-9849-3, 2013.

831 Williams, A. G., Zahorowski, W., Chambers, S., Griffiths, A., Hacker, J. M., Element, A. and
832 Werczynski, S.: The Vertical Distribution of Radon in Clear and Cloudy Daytime Terrestrial
833 Boundary Layers, J. Atmos. Sci., 68(1), 155–174, doi:10.1175/2010JAS3576.1, 2010.

834 Xu, X., Werner, M., Butzin, M. and Lohmann, G.: Water isotope variations in the global ocean
835 model MPI-OM, Geosci. Model Dev., 5(3), 809–818, doi:10.5194/gmd-5-809-2012, 2012.

836 Zahorowski, W., Chambers, S. D. and Henderson-Sellers, A.: Ground based radon-222
837 observations and their application to atmospheric studies, J. Environ. Radioact., 76(1–2), 3–33,
838 doi:http://dx.doi.org/10.1016/j.jenvrad.2004.03.033, 2004.

839 Zhao, L., Wang, L., Liu, X., Xiao, H., Ruan, Y. and Zhou, M.: The patterns and implications of
840 diurnal variations in the d-excess of plant water, shallow soil water and air moisture, Hydrol. Earth
841 Syst. Sci., 18(10), 4129–4151, doi:10.5194/hess-18-4129-2014, 2014.

Hydrol. Earth Syst. Sci. Discuss., doi:10.5194/hess-2016-271, 2016
Manuscript under review for journal Hydrol. Earth Syst. Sci.
Published: 30 June 2016

842

843 **8 Figure Captions**

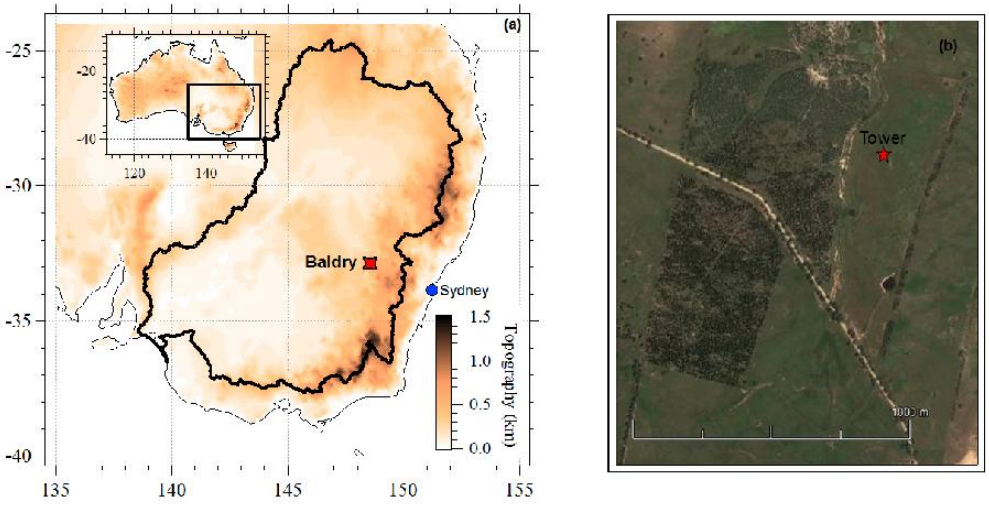

844

Figure 1: a) Location of the Baldry Hydrological Observatory, the heavy black border shows the limits of the Murray-Darling Basin, (b) location of the field site used for the campaign.

845

Hydrol. Earth Syst. Sci. Discuss., doi:10.5194/hess-2016-271, 2016
Manuscript under review for journal Hydrol. Earth Syst. Sci.
Published: 30 June 2016

Hydrology and Earth System Sciences
Discussions

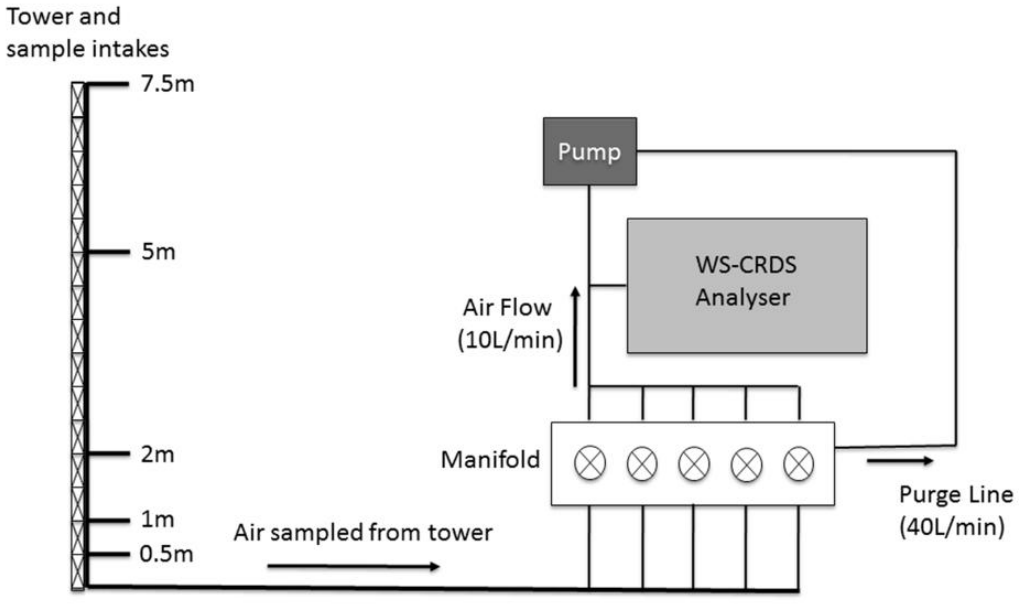

846

847 Figure 2: Sampling system for the automated in-situ sampling of water vapour isotopes from the

848 tower.

Hydrol. Earth Syst. Sci. Discuss., doi:10.5194/hess-2016-271, 2016
Manuscript under review for journal Hydrol. Earth Syst. Sci.
Published: 30 June 2016

849

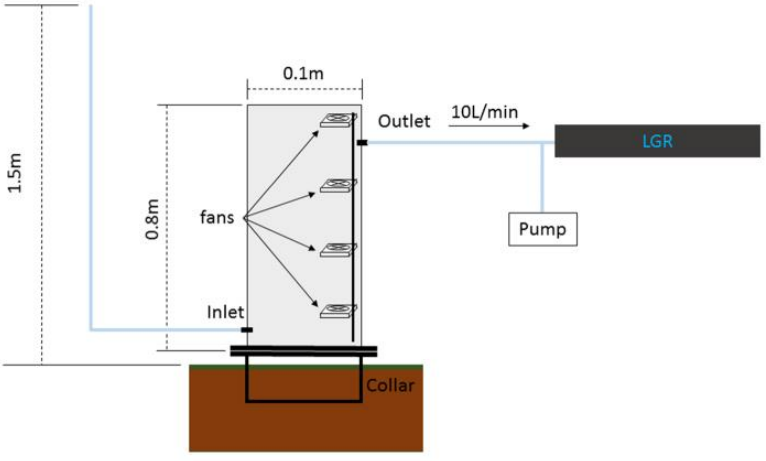

850

851 Figure 3: Chamber design used for determining isotopic compositions of ET fluxes.

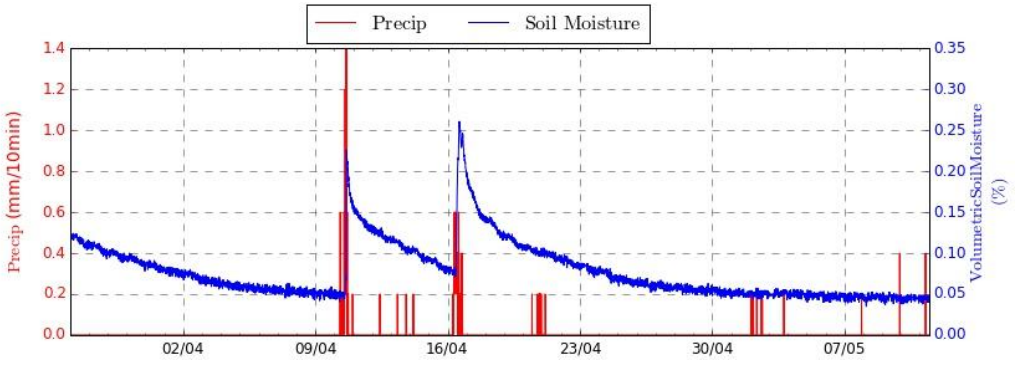

852

Hydrol. Earth Syst. Sci. Discuss., doi:10.5194/hess-2016-271, 2016
Manuscript under review for journal Hydrol. Earth Syst. Sci.
Published: 30 June 2016

Hydrology and Earth System Sciences
Discussions

Figure 4: Precipitation and 0-10 cm soil moisture for the month leading up to and including the field campaign.

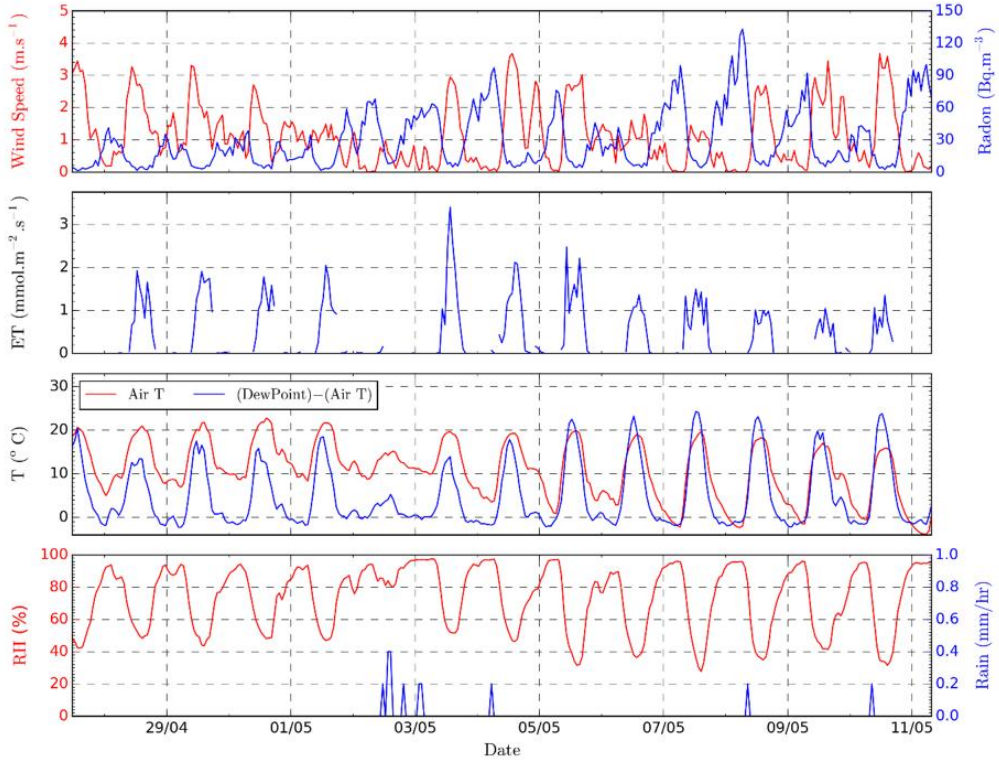

853

Figure 5: Meteorological and radon measurements collected throughout the field campaign. Meteorological measurements are block hourly averages calculated from 15-minute observations. Small rain events on the 4th, 8th and 10th May were most likely dew fall rather than precipitation.

854

Hydrol. Earth Syst. Sci. Discuss., doi:10.5194/hess-2016-271, 2016
Manuscript under review for journal Hydrol. Earth Syst. Sci.
Published: 30 June 2016

Hydrology and Earth System Sciences
Discussions

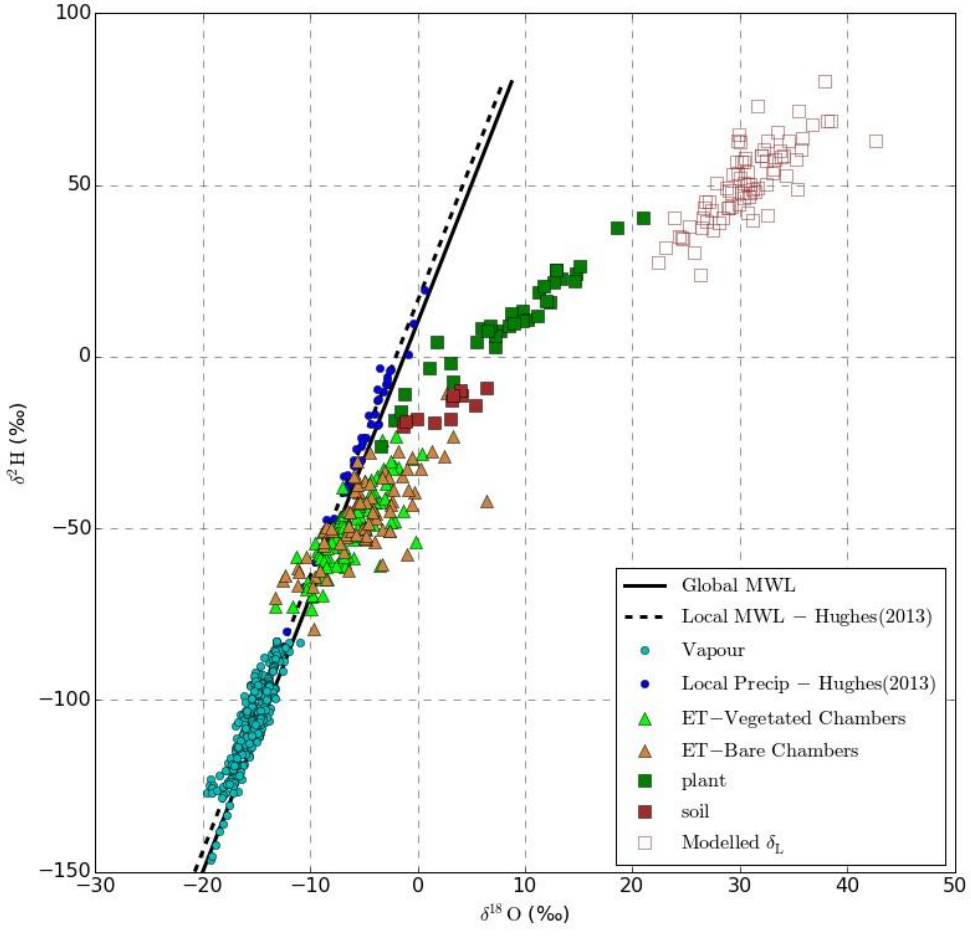

855

Figure 6: Relationship between δ^2H and δ^{18}O for observed and modelled water pools. Linear regressions are shown for local and global meteoric water lines (MWL). Data from Hughes and Crawford (2013) are for monthly cumulative rainfall samples between 2005 and 2008.

856

Hydrol. Earth Syst. Sci. Discuss., doi:10.5194/hess-2016-271, 2016
Manuscript under review for journal Hydrol. Earth Syst. Sci.
Published: 30 June 2016

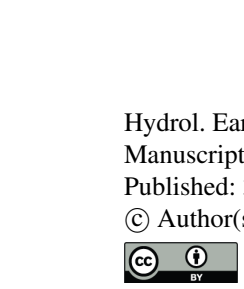

Hydrology and Earth System Sciences
Open Access
Discussions

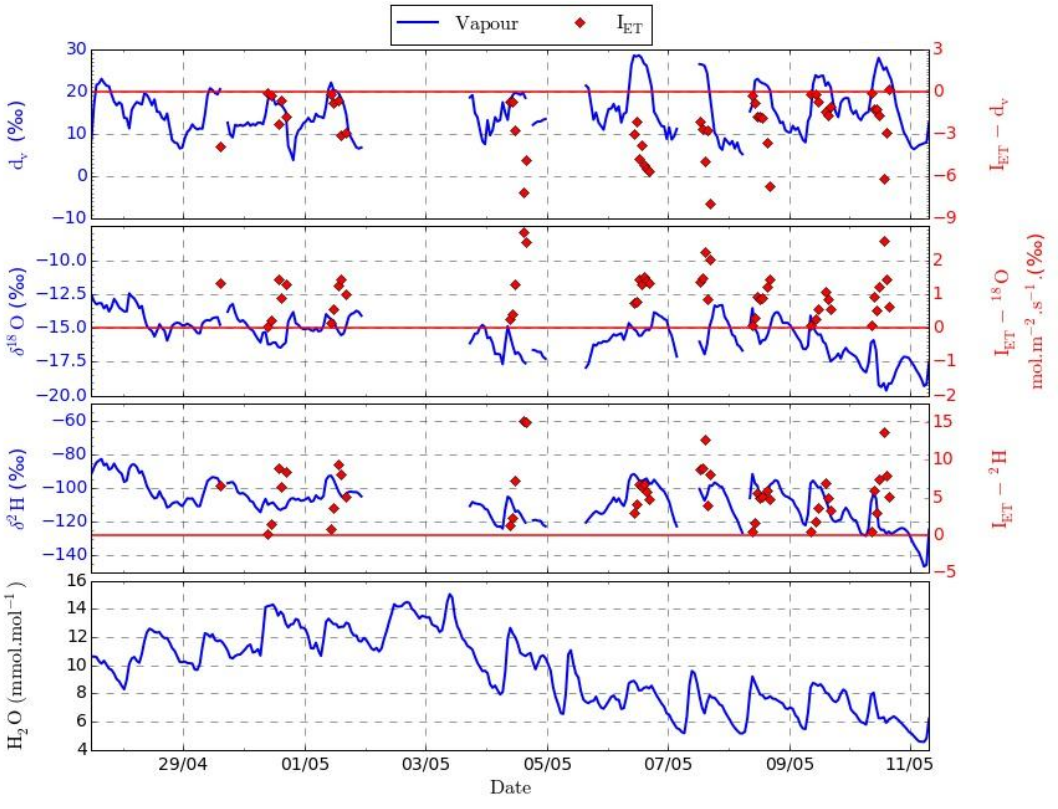

857

Figure 7: Time series of hourly water vapour mixing ratio, isotopic composition and ET iso-forcing (I_{ET}).

858

Hydrol. Earth Syst. Sci. Discuss., doi:10.5194/hess-2016-271, 2016
Manuscript under review for journal Hydrol. Earth Syst. Sci.
Published: 30 June 2016

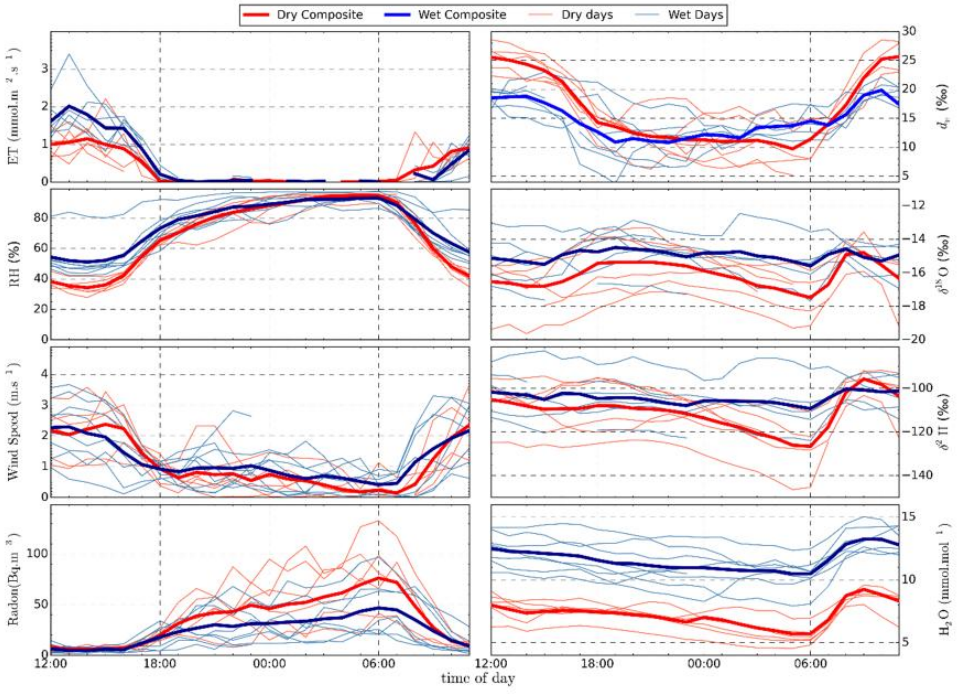

859

Figure 8: Data plotted by time of day and divided into dry and wet periods (see text in section 3.5). Diurnal composites are shown for dry (red) and wet (blue) periods.

860

Hydrol. Earth Syst. Sci. Discuss., doi:10.5194/hess-2016-271, 2016
Manuscript under review for journal Hydrol. Earth Syst. Sci.
Published: 30 June 2016

Hydrology and Earth System Sciences
Discussions

Table 1: Correlation between meteorological variables and the isotopic composition of water vapour. Values outside the brackets are statistics for the hourly observations. Inside the brackets are correlation statistics for average values calculated between 11:00 and 15:00 LST, hence representing activity during a convective boundary layer. Significant correlation are shown in bold; $p<0.001$ for hourly observations and $p<0.05$ for the daytime averages (due to the smaller number of points).

		T	RH	ET	H_2O	I_{ET}[a]
δ^2H	**Slope**	**0.83** (0.51)	**-0.17** (0.23)	1.4 (6.1)	**2.1** (0.85)	-1.1 **(-3.0)**
	Intercept	**-120** (-140)	**-95** (-110)	-110 (-110)	**-110** (-130)	-99 **(-83)**
	R^2	**0.24** (0.13)	**0.09** (0.02)	0.001 (0.04)	**0.2** (0.04)	0.2 **(0.45)**
	p	**<0.001** (0.3)	**<0.001** (0.7)	0.32 (0.6)	**<0.001** (0.5)	0.002 **(0.05)**
$\delta^{18}O$	**Slope**	**0.046** (0.44)	-0.01 (-0.01)	-0.37 (1.8)	**0.27** (0.29)	-0.7 (-1.9)
	Intercept	**-16** (-24)	-16 (-20)	-15 (-18)	**-18** (-19)	-15 (-14)
	R^2	**0.04** (0.30)	0.004 (0.2)	0.02 (0.16)	**0.2** (0.2)	0.14 (0.32)
	p	**<0.001** (0.08)	0.26 (0.19)	0.05 (0.26)	**<0.001** (0.15)	0.008 (0.11)
d_v	**Slope**	**0.51 (-1.4)**	**-0.21 (-0.52)**	0.01 **(-0.16)**	0.15 **(-1.3)**	-1.4 (-2.4)
	Intercept	**-9.9 (48)**	**31 (44)**	-15 **(-18)**	14 **(35)**	21 (20)
	R^2	**0.40 (0.48)**	**0.62 (0.74)**	0.22 **(0.30)**	0.004 **(0.71)**	0.06 (0.08)
	p	**<0.001** (**0.02**)	**<0.001** (**<0.01**)	0.05 **(0.01)**	0.26 **(<0.01)**	0.01 (0.44)

[a]Iso-forcing correlations were calculated for simultaneous vapour and chamber measurements. Hourly averaged values were used for both.